

Sheath-Less Dielectrophoresis-Based Microfluidic Chip for Label-Free Bio-Particle Focusing and Separation [†]

Reza Vamegh ¹, Zeynab Alipour ^{1,*} and Mehdi Fardmanesh ¹

¹ Department of Electrical Engineering, Sharif University of Technology, Azadi Avenue, Tehran P.O. Box 11365-8639, Iran; reza.vamegh@ee.sharif.edu (R.V.); fardmanesh@sharif.edu (M.F.)

* Correspondence: alipour_zeynab@ee.sharif.edu

[†] Presented at the 10th International Electronic Conference on Sensors and Applications (ECSA-10), 15–11 30 November 2023; Available online: <https://ecsa-10.sciforum.net/>.

Abstract: This paper presents a novel microfluidic dielectrophoresis (DEP) system to focus and separate cells of similar size based on their structural differences, which is more challenging than separation by size. Because, in this case, the DEP force is only proportional to the polarizabilities of cells. We used live and dead yeast cells as bioparticles to investigate the chip efficiency. Our designed chip consists of three sections. First, focusing cells in the center of the microchannel by employing a negative DEP phenomenon. After that, cells are separated due to the different deflection from high electric field areas. Finally, a novel outlet design was utilized to facilitate separation by increasing the gap between the two groups of cells. The proposed sheath-free design has one inlet for target cell injection requiring only one pump to control the flow rate, which reduces costs and complexity. Successful discrimination of the particles was achieved by using DEP force as a label-free and highly efficient technique. As an accessible and cost-effective method, soft lithography by 3D printed resin mold was used to fabricate microfluidic parts. Microchannel is made of Polydimethylsiloxane (PDMS) material that is biocompatible. The electrodes are made of gold due to its biocompatibility and non-oxidation, and a titanium layer is sputtered as the buffer layer for the adhesion of the sputtered gold layer to the glass. A standard microfabrication process is employed to create the electrode pattern. O₂ plasma treatment yielded a leakage-free bonding between patterned glass and PDMS structure containing microfluidic channel. The maximum voltage applied to the electrodes (26 V) is lower than the threshold value for cell electroporation. Simulations and experimental results both confirm the effectiveness of the proposed microfluidic chip.

Keywords: Dielectrophoresis; Microfluidics; Planar electrodes; Cell separation; Active focusing

Citation: Vamegh, R.; Alipour, Z.; Fardmanesh, M. Sheath-Less Dielectrophoresis-Based Microfluidic Chip for Label-Free Bio-Particle Focusing and Separation. *Sensors* **2023**, *5*, x. <https://doi.org/10.3390/xxxxx>

Academic Editor(s):

Published: 15 November 2023



Copyright: © 2023 by the authors. Submitted for possible open access publication under the terms and conditions of the Creative Commons Attribution (CC BY) license (<https://creativecommons.org/licenses/by/4.0/>).

1. Introduction

Microfluidics is a rapidly growing field that concerns the manipulation and study of minute amounts of fluids flowing through microchannels [1]. Due to its precise control over fluids, microfluidics presents unique features, including reduced sample size requirements, enhanced speed and sensitivity, and the ability to integrate multiple analytical and laboratory functions onto a single chip [2]. This interdisciplinary technology has led to astonishing advances in various domains, including drug discovery [3], medical diagnostics [4], biosensing [5], environmental monitoring [6], and food safety [7].

The ability to analyze cells is the cornerstone of numerous scientific investigations, including diagnostic and therapeutic applications and biomedical research. The study of cells provides essential information on their structure, function, and behavior and aids in understanding the physiology of organisms. The information obtained through cell analysis has significant applications in fields like oncology, neurology, and immunology [8]. In this regard, isolating specific cell populations from a heterogeneous sample with high

purity and yield is a vital step in several experimental protocols [9]. Cell separation processes are necessary for gene expression analysis, proteomics, and cell-based therapies.

The combination of microfluidics and cell separation has unlocked new prospects in studying intricate cellular processes. Based on their operational principles, microfluidic cell separation techniques can be classified into passive and active methods [10]. Passive methods harness the power of meticulous channel structures, hydrodynamic forces, and steric interactions to manipulate particles via various mechanisms, such as deterministic lateral displacement (DLD) [11], pinch flow fractionation (PFF), hydrodynamic filtration, inertial and secondary flow [12]. Conversely, active microfluidic separation methods rely on external fields to propel particles toward specific locations for separation. Fluorescence-activated cell sorting (FACS) [13], acoustophoresis [14], magnetophoresis [15], and dielectrophoresis (DEP) [16] are some of these active methods.

One of the most prominent microfluidic cell separation techniques is the DEP separation method, a non-invasive and label-free approach. Its high flexibility ensures the selective manipulation of cells based on their diverse bio-physical characteristics, including size, shape, and dielectric properties. Moreover, it is highly proficient in processing large volumes of cells, resulting in high-purity samples with exceptional throughput. Lastly, DEP is a highly versatile tool that can integrate with other microfluidic techniques, including microfluidic imaging, single-cell analysis, and microfluidic sensors [17,18].

In this work, we present the design and fabrication of an integrated microfluidic chip capable of separating cells of similar size based on their structural differences via the DEP mechanism. The novel feature of our microchip lies in utilizing a single applied frequency to achieve cell focusing without using sheath flows and separation while positioning electrodes on both sides of the microchannel. We used the negative DEP phenomenon to narrow the streamline of cells in the middle of the microchannel. Hence, all cells experienced the same electric field with the sole differentiating factor being the structural-based variation in the DEP forces they encountered. The subtle arrangement and size of the focusing and separating microelectrodes attained the optimal non-uniformity of the electric field while minimizing voltage requirements to promote cell viability. Our easy, low-cost, and rapid fabrication method allows cost-effective mass production of our device. We simulated flow field distribution, electric field distribution, and particle trajectories to optimize the device operation. Finally, we validated our microchip's performance by conducting experiments using live and dead yeast cells as bioparticles with similar sizes.

2. Materials and Methods

2.1. Theoretical Background

The DEP phenomenon occurs when non-uniform electric fields interact with neutral particles possessing a dipole moment. When such particles are placed in an inhomogeneous electric field, charges will start accumulating at the interface between the medium and the particle, creating dipoles that interact with the electric field. Consequently, the particles undergo a net force and begin to move. The fundamental principle of DEP relies on the difference in polarizabilities between the particles and their suspending medium. If the particle has a higher polarizability than the medium, it will experience a net force towards areas of high electric field. Conversely, if the particle's polarizability is lower than the medium, the DEP force will be directed in the opposite direction.

Utilizing the dipole moment method on a homogenous spherical particle of radius r suspended in a dielectric medium with permittivity ϵ_m , the time-average DEP force acting on the particle can be determined [19]:

$$\langle \vec{F}_{DEP}(t) \rangle = 2\pi\epsilon_m r^3 \text{Re}\{f_{CM}(\omega)\} \nabla E_{rms}^2 \quad (1)$$

where $\text{Re}\{ \}$ is the real part of a complex number, E_{rms} is the root mean square of the applied electric field, and $f_{CM}(\omega)$ is the Clausius–Mossotti factor [19]:

$$f_{CM}(\omega) = \frac{\epsilon_p^*(\omega) - \epsilon_m^*(\omega)}{\epsilon_p^*(\omega) + 2\epsilon_m^*(\omega)} \tag{2}$$

where $\epsilon_p^*(\omega)$ and $\epsilon_m^*(\omega)$ are effective complex permittivity of particle and medium, respectively that is given by $\epsilon - j\sigma/\omega$, where ϵ is the permittivity of the material, σ is the material conductivity, and ω is the angular frequency.

From the DEP force equation, it is evident that the DEP force direction depends on the sign of $\text{Re}\{f_{CM}(\omega)\}$. When $\text{Re}\{f_{CM}(\omega)\} > 0$, the DEP force acts in the direction of the high electric field, causing the particle to be attracted towards the field's region, which is called positive DEP (PDEP). Conversely, for $\text{Re}\{f_{CM}(\omega)\} < 0$, particles are deflected from the region of higher field intensity to a lower one, known as negative DEP (NDEP).

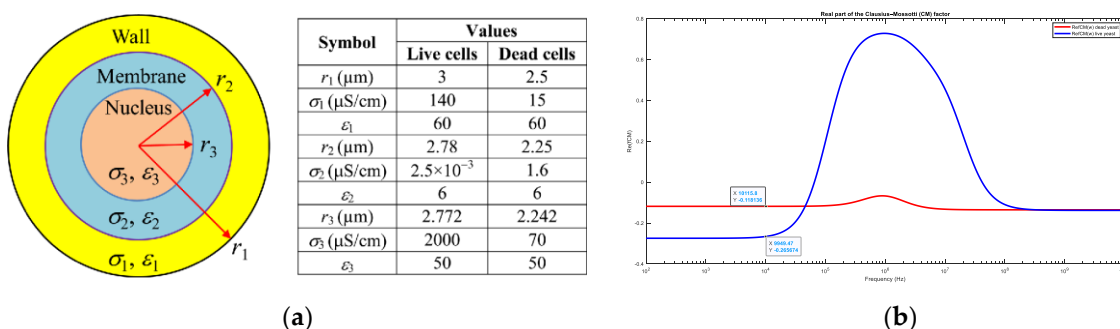


Figure 1. Yeast cells, (a) Two-shell model [20] (b) Calculated $\text{Re}\{f_{CM}(\omega)\}$ for Live and dead yeast cells.

Using the two-shell model (Figure 1a) for live and dead yeasts [20], we plotted the $\text{Re}\{f_{CM}(\omega)\}$ (Figure 1b) and determined 10 kHz as our optimal operating frequency.

2.2. Design and Simulation

Figure 2 presented herein illustrates our novel and inventive design strategy:

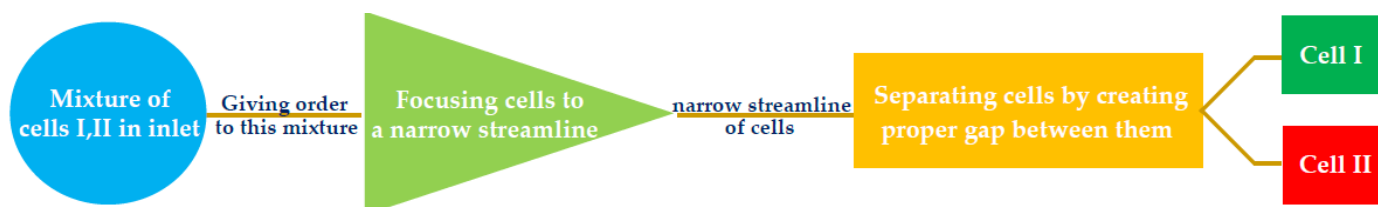


Figure 2. Strategy to design microfluidic DEP-based chip for cell separation.

Our initial objective aimed to ensure that all cells experienced the same electric field. We leveraged the NDEP phenomenon to cause the movement of particles in the same direction toward low-field regions by applying a frequency of 10 kHz to the focusing electrodes. To facilitate the concentration process and reduce the required applied voltage, we began with a smaller section with a width of 50 microns that gradually widened to 100 microns. At the 100-micron segment, we employed two sets of four electrodes to concentrate the cells towards the center of the microchannel. The width of the upper electrodes was 120 microns (Figure 3a), while the lower electrodes had an 80-micron width, creating the desired non-uniform field. Figure 3b shows the overall performance of the focusing section consisting of three subsections with a total length of 3400 microns.

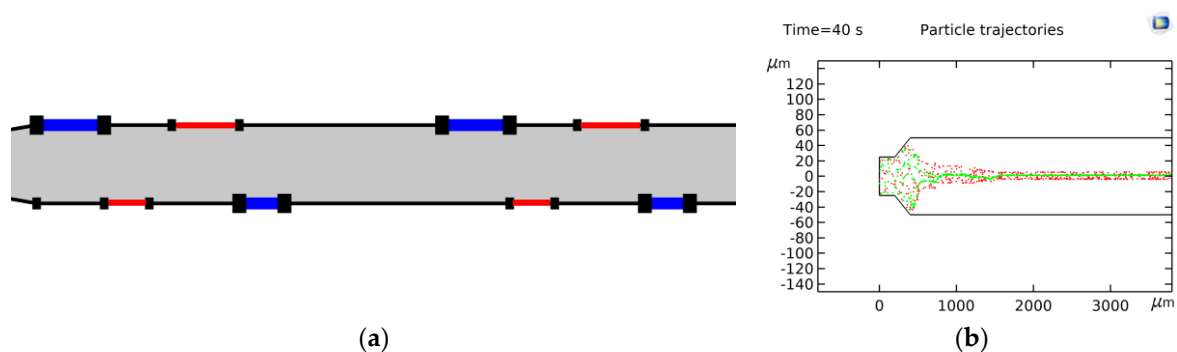


Figure 3. Focusing section, (a) Electrode arrangement (b) Overall performance.

After cell focusing, we went on to separate the cells by gradually increasing the gap between viable (green) and nonviable (red) cells using the NDEP. The separation section was carefully optimized to ensure maximum distance between the two clusters of cells, utilizing a 10:1 size ratio for the electrodes in an arrangement that caused the particles' trajectory to oscillate about the channel's symmetry axis. In the final part of the separation section, we incorporated a step increase in the channel width to ease separation by widening the gap between the two groups of cells. Through further simulations and optimizations, we determined that 26 volts is the minimum operating voltage for both focusing and separation electrode pairs, with the red electrodes grounded. Figure 4a displays the electric field intensity over the entire structure. Moreover, Figure 4b shows the particles' trajectory near the outlets with a 37-micron gap between the two cell groups.

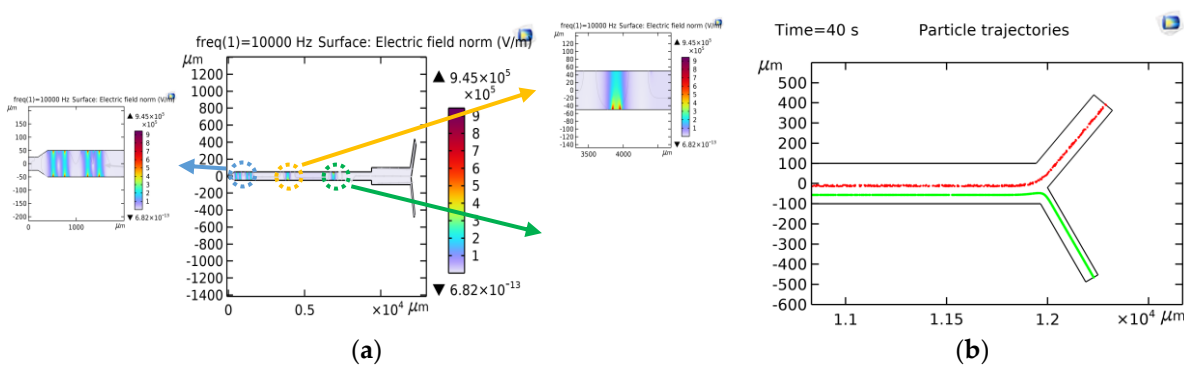


Figure 4. Optimized structure, (a) Electric field distribution (b) Particles' trajectory near the outlets.

2.3. Fabrication

Figure 5 represents the fabrication steps comprising three phases: microelectrode formation on glass, microfluidic channel creation, and bonding. Gold was selected for the microelectrodes due to its suitable electrical conductivity, non-oxidizing properties, and biocompatibility. A sputtering process is employed to deposit a titanium layer to improve the adhesion of gold to glass, followed by Au layer deposition. To form the pattern of our microelectrodes, we performed standard photolithography by utilizing S1813 positive photoresist. Afterward, the excessive Au and Ti were etched, leaving only the microelectrode details. For the microfluidic part, we employed soft lithography, which involved using an LCD 3D printer to produce a 3D-printed mold to cast PDMS. Subsequently, the resulting microchannel part was cured and perforated for inlet and outlet ports. Next, we plasma-bonded the PDMS-based microchannel part to the patterned substrate containing electrodes to form an integrated microfluidic chip. Lastly, the inlet and outlet hoses were placed.

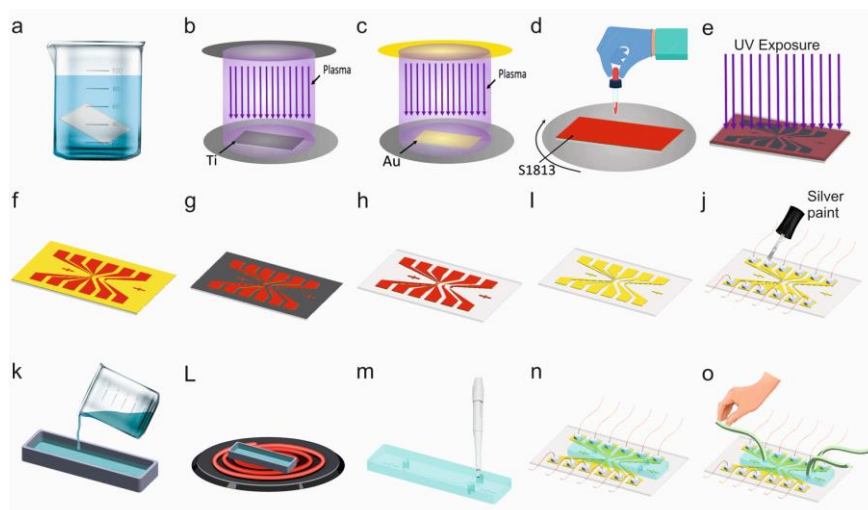


Figure 5. Fabrication Process, (a) Cleaning glass substrate in acetone and isopropyl alcohol (IPA), (b) DC plasma sputtering of titanium layer, (c) DC plasma sputtering of Au layer, (d) Spin coating S1813 positive photoresist, (e) Photolithography process for electrodes patterning, (f) Developing excessive photoresist in the NaOH, (g) Etching the gold layer, (h) Etching the Ti layer, (i) Removing the photoresist using acetone, (j) Placing the electrical contact wires using the silver paint, (k) Pouring the PDMS in the 3d printed mold for microchannel part, (l) Curing the PDMS on the hotplate for 60 min at 80 °C, (m) Punching the inlet and outlet ports, (n) Plasma bonding the PDMS-based microchannel part to the substrate containing electrodes, (o) Placing inlet and outlet hoses.

Figure 6 shows the integrated microfluidic chip.

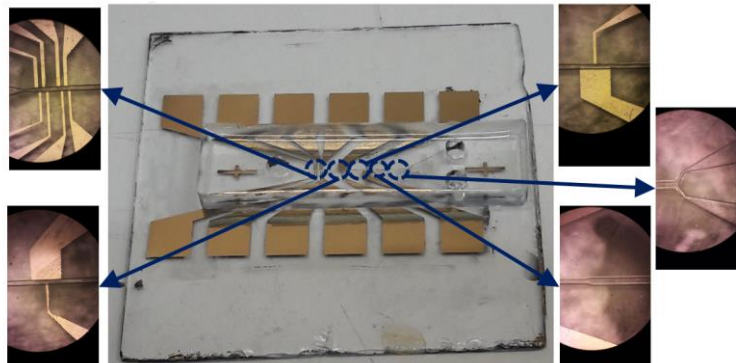


Figure 6. Fabricated chip structure.

2.4. Sample Preparation

Since we wanted to develop a yeast solution with minimal electrical conductivity, we chose deionized water as the base solvent. Initially, we heated 50 milliliters of deionized water to 40 °C for 30 min, followed by the addition of 3.5 g of sugar, which we stirred to dissolve. We then added 1.5 g of dry yeast powder and stirred the solution. The resulting solution containing cells was diluted in a 1:4 ratio with the base sugar water solution. We subjected half of the original yeast solution to a temperature of 100 °C for 30 min to obtain a solution with dead yeast cells.

Using the electrochemical impedance spectroscopy (EIS) system, we determined the relative permittivity and conductivity of the base solution as 243.6 and 78.64 $\mu\text{S}/\text{cm}$.

3. Results and Discussion

The results presented in Figures 7a–c exhibit the successful implementation of particle focusing through using the NDEP phenomenon. After entering the channel and passing through the two pairs of concentrating electrodes, each consisting of four electrodes,

cells are positioned in the center of the microchannel. By exploiting the NDEP phenomenon, particles tend to migrate toward regions with lower electric field intensity, experiencing oscillatory and sinusoidal motion along the channel's symmetry axis before ultimately settling at the microchannel centerline.

Figures 7d and 7e indicate the cells' trajectory near the first and second separating electrodes, respectively. As observed, particles move away from small electrodes where electric field lines accumulate and move towards the lower electric field intensity regions.

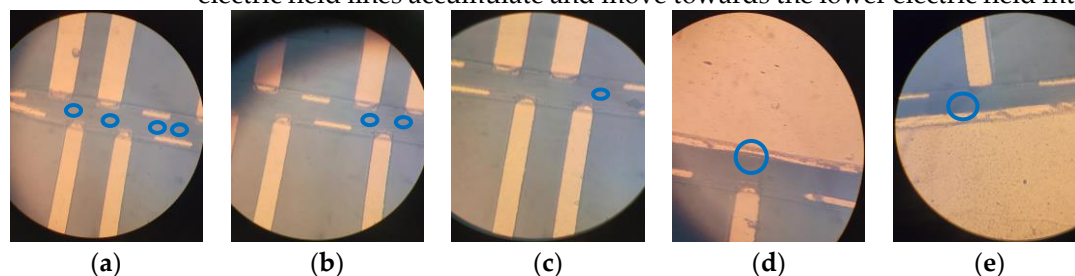


Figure 7. Particle's trajectories (cells are marked in blue circles), (a) near 1st focusing pair, (b) between 1st and 2nd focusing pair, (c) near 2nd focusing pair, (d) near 1st separating pair, (e) near 2nd separating pair.

4. Conclusions

We introduced an integrated microfluidic chip for separating bio-particles of similar size. Our innovative microelectrode design and microchannel architecture enable precise separation of cells based on their distinct dielectric properties. Leveraging a single frequency in our microelectrode configuration, we achieved exceptional efficiency and accuracy in sorting bio-particles. Our microfluidic chip comprises two parts—a focuser and a separator. Our NDEP force-driven focuser actively aligns particles in the center of the channel without any additional pump or sheath flow. We employed an electric field of 26 volts at a 10 kHz frequency to accomplish this task. In the separator part, we utilized the NDEP phenomenon to separate particles through varying deviations in the electric field, using the electric field conditions as the focuser part. Through a step increase in channel width, we maximized the gap between the two target particles to improve the effectiveness of the separation process. Our microdevice is easy to fabricate, requires low voltage, and is compatible with many types of cells, making it an attractive option for research and clinical applications. Our novel chip design has the potential to drastically change the existing cell separation methods, opening the door for further advancements in various fields of life sciences and biomedical research.

Author Contributions: Conceptualization, Z.A.; methodology, Z.A. and R.V.; software, R.V.; validation, R.V., Z.A., and M.F.; investigation, Z.A. and R.V.; resources, M.F.; data curation, R.V. and Z.A.; writing—original draft preparation, R.V. and Z.A.; writing—review and editing, R.V., Z.A., and M.F.; visualization, R.V., Z.A., and M.F.; supervision, M.F.; project administration, Z.A.; All authors have read and agreed to the published version of the manuscript.

Funding: This research received no external funding.

Institutional Review Board Statement: Not applicable.

Informed Consent Statement: Not applicable.

Conflicts of Interest: The authors declare no conflict of interest.

References

- Whitesides, G.M. The origins and the future of microfluidics. *Nature* **2006**, *442*, 368–373. <https://doi.org/10.1038/nature05058>.
- Bahnemann, J.; Grünberger, A. Microfluidics in Biotechnology: Overview and Status Quo. *Adv. Biochem. Eng. Biotechnol.* **2022**, *179*, 1–16. https://doi.org/10.1007/10_2022_206.
- Liu, Y.; Sun, L.; Zhang, H.; Shang, L.; Zhao, Y. Microfluidics for Drug Development: From Synthesis to Evaluation. *Chem. Rev.* **2021**, *121*, 7468–7529. <https://doi.org/10.1021/acs.chemrev.0c01289>.

4. Chandra M. Pandey, B.D.M.; Augustine, S.; Kumar, S.; Nara, S.; Srivastava, S. Microfluidics Based Point-of-Care Diagnostics. *Biotechnol J.* **2018**, *13*, 1700047. <https://doi.org/10.1002/biot.201700047>.
5. Kulkarni, M.B.; Ayachit, N.H.; Aminabhavi, T.M. Biosensors and Microfluidic Biosensors: From Fabrication to Application. *Biosensors* **2022**, *12*, 543. <https://doi.org/10.3390/bios12070543>.
6. Pol, R.; Céspedes, F.; Gabriel, D.; Baeza, M. Microfluidic lab-on-a-chip platforms for environmental monitoring. *TrAC-Trends Anal. Chem.* **2017**, *95*, 62–68. <https://doi.org/10.1016/j.trac.2017.08.001>.
7. Mu, R.; Bu, N.; Pang, J.; Wang, L.; Zhang, Y. Recent Trends of Microfluidics in Food Science and Technology: Fabrications and Applications. *Foods* **2022**, *11*, 3727. <https://doi.org/10.3390/foods11223727>.
8. Christodoulou, M.I.; Zaravinos, A. Single-Cell Analysis in Immuno-Oncology. *Int. J. Mol. Sci.* **2023**, *24*, 1–19. <https://doi.org/10.3390/ijms24098422>.
9. Hu, P.; Zhang, W.; Xin, H.; Deng, G. Single cell isolation and analysis. *Front. Cell Dev. Biol.* **2016**, *4*, 1–12. <https://doi.org/10.3389/fcell.2016.00116>.
10. Shiri, F.; Feng, H.; Gale, B.K. Passive and active microfluidic separation methods. Elsevier: Amsterdam, The Netherlands, 2022.
11. Sherbaz, A.; Konak, B.M.K.; Pezeshkpour, P.; Di Ventura, B.; Rapp, B.E. Deterministic Lateral Displacement Microfluidic Chip for Minicell Purification. *Micromachines* **2022**, *13*, 365. <https://doi.org/10.3390/mi13030365>.
12. Zhao, Q.; Yuan, D.; Zhang, J.; Li, W. A review of secondary flow in inertial microfluidics. *Micromachines* **2020**, *11*, 1–23. <https://doi.org/10.3390/MII11050461>.
13. Drescher, H.; Weiskirchen, S.; Weiskirchen, R. Flow cytometry: A blessing and a curse. *Biomedicines* **2021**, *9*, 1–12. <https://doi.org/10.3390/biomedicines9111613>.
14. Yang, A.H.J.; Soh, H.T. Acoustophoretic sorting of viable mammalian cells in a microfluidic device. *Anal. Chem.* **2012**, *84*, 10756–10762. <https://doi.org/10.1021/ac3026674>.
15. Poudineh, M.; Sargent, E.H.; Pantel, K.; Kelley, S.O. Profiling circulating tumour cells and other biomarkers of invasive cancers. *Nat. Biomed. Eng.* **2018**, *2*, 72–84. <https://doi.org/10.1038/s41551-018-0190-5>.
16. Valijam, S.; Salehi, A.; Andersson, M. Design of a low-voltage dielectrophoresis lab-on-the chip to separate tumor and blood cells. *Microfluid. Nanofluidics* **2023**, *27*, 1–11. <https://doi.org/10.1007/s10404-023-02632-9>.
17. Zhang, H.; Chang, H.; Neuzil, P. DEP-on-a-chip: Dielectrophoresis applied to microfluidic platforms. *Micromachines* **2019**, *10*, 1–22. <https://doi.org/10.3390/mi10060423>.
18. Pesch, G.R.; Du, F. A review of dielectrophoretic separation and classification of non-biological particles. *Electrophoresis* **2021**, *42*, 134–152. <https://doi.org/10.1002/elps.202000137>.
19. Gascoyne, P.R.C.; Vykoukal, J. Particle separation by dielectrophoresis. *Electrophoresis* **2002**, *23*, 1973–1983. [https://doi.org/10.1002/1522-2683\(200207\)23:13<1973::AID-ELPS1973>3.0.CO;2-1](https://doi.org/10.1002/1522-2683(200207)23:13<1973::AID-ELPS1973>3.0.CO;2-1).
20. Patel, S.; Showers, D.; Vedantam, P.; Tzeng, T.R.; Qian, S.; Xuan, X. Microfluidic separation of live and dead yeast cells using reservoir-based dielectrophoresis. *Biomicrofluidics* **2012**, *6*, 1–12. <https://doi.org/10.1063/1.4732800>.